optics

MDPI

Article

Shortwave near Infrared–Hyperspectral Imaging Spectra to Detect Pork Adulteration in Beef Using Partial Least Square Regression Coupled with VIP Wavelength Selections Method

Rudiati Evi Masithoh [1,*], Reza Adhitama Putra Hernanda [2], Muhammad Fahri Reza Pahlawan [3], Juntae Kim [4], Hanim Zuhrotul Amanah [1] and Byoung-Kwan Cho [3,4]

[1] Department of Agricultural and Biosystems Engineering, Faculty of Agricultural Technology, Universitas Gadjah Mada, Yogyakarta 55281, Indonesia; hanim_za@ugm.ac.id
[2] Department of Biosystems Engineering, College of Agriculture, Life and Environment Science, Chungbuk National University, Chungdae-ro, Seowon-gu, Cheongju 28644, Republic of Korea; reza.a.p@chungbuk.ac.kr
[3] Department of Smart Agriculture Systems, College of Agricultural and Life Science, Chungnam National University, Daejeon 34134, Republic of Korea; freza836@gmail.com (M.F.R.P.); chobk@cnu.ac.kr (B.-K.C.)
[4] Department of Biosystems Machinery Engineering, College of Agricultural and Life Science, Chungnam National University, Daejeon 34134, Republic of Korea; biosch94@gmail.com
* Correspondence: evi@ugm.ac.id

Abstract: Pork adulteration detection in beef is important due to health, economic, and religious concerns. This study explored the use of a Shortwave Near Infrared–Hyperspectral Imaging (SWNIR–HSI) system which captured spectral data across 894–2504 nm to detect adulteration of pork in beef. In this study, minced pork in various concentrations ranging from 0–50% (*w*/*w*) were added to pure minced beef. Spectra obtained from the SWNIR–HSI were used to develop a partial least square regression (PLSR) model. The study compared the PLSR results between full wavelengths (variables) and selected wavelengths obtained via the variable importance in projection (VIP) method. The best results from the full-wavelength PLSR model yielded a prediction accuracy (R^2P) of 0.940 and a standard error of prediction (SEP) of 4.633%, while using VIP-selected wavelengths improved performance, with R^2P of 0.955 and SEP of 3.811%. The study demonstrates the potency of SWNIR–HIS, particularly with selected wavelengths, as an effective and nondestructive tool for accurately predicting pork adulteration levels in beef.

Keywords: pork; beef; adulteration; hyperspectral imaging (HSI); shortwave near-infrared (SWNIR); partial least square regression (PLSR); variable importance in projection (VIP)

Academic Editor: Francesco Chiavaioli

Received: 1 November 2024
Revised: 18 December 2024
Accepted: 31 December 2024
Published: 3 January 2025

Citation: Masithoh, R.E.; Hernanda, R.A.P.; Pahlawan, M.F.R.; Kim, J.; Amanah, H.Z.; Cho, B.-K. Shortwave near Infrared–Hyperspectral Imaging Spectra to Detect Pork Adulteration in Beef Using Partial Least Square Regression Coupled with VIP Wavelength Selections Method. *Optics* **2025**, *6*, 1. https://doi.org/10.3390/opt6010001

1. Introduction

Food adulteration is a form of food fraud that is intentionally conducted to reduce food quality, misrepresenting brand, origin, ingredients, and composition [1]. In the case of meat adulteration, this usually involves adding other meat products, for example, the addition of pork into beef or lamb [2,3], horsemeat into beef [4], or pork and duck into beef [5]. Meat adulteration brings about serious concerns, especially among consumers and within the industry. Adulteration leads to foodborne illnesses due to the consumption of unapproved substances and allergens [6]. It also causes economic losses if low-priced meat is sold as a high-priced product. In addition to health and financial concerns, meat adulteration results in religious concerns [2]; for example, Muslims do not allow pork consumption and Hindus do not allow beef consumption. Therefore, developing reliable and efficient methods to detect meat adulteration is important.

Detection of adulteration in food and agricultural products has been extensively studied using sensory, chemical, chromatographic, and spectral methods. Sensory analysis was used to detect adulteration in honey by sugar syrup [7] or Shiikuwasha Juice [8]. Chemical markers can also be used to detect adulteration or authentication using gas or liquid chromatography [9]. Conventional and real-time polymerase chain reaction (PCR) was used to detect adulteration in honey [10] and milk [7]. However, considering practical aspects, these methods have some limitations, such as being destructive, time-consuming, requiring skillful operation, and producing chemical waste, despite being accurate. To overcome the limitations of these conventional methods, employing an optical technique, such as spectroscopy, is likely to be more favorable, allowing rapid and nondestructive measurement. The principle behind spectroscopy techniques ais based on the unique response of molecules within any sample due to the present of light. In agriculture, measurement between ultraviolet (UV) and infrared (IR) regions has been intensively used, due to the fact that agricultural materials are detectable in these regions. For instance, visible–near infrared (Vis–NIR), near-infrared (NIR), and mid-infrared (MIR) spectroscopies have been successfully used to identify the presence of adulterants in various food materials: palm sugar [11–13], meat [3], and various types of tuber flour [14]. Another study demonstrated the potency of Raman spectroscopy, measuring from 200 to 1800 cm^{-1}, in predicting crude fat and protein contents in soybean [15].

Conventional IR spectroscopy provides a mean spectrum for a sample as a single spectrum; thus, the sample loses the spatial distribution of constituent information within the sample. Furthermore, conventional spectroscopy techniques are relatively time consuming, since the measurement is carried out one-by-one. IR hyperspectral imaging (IR–HSI), which combines IR spectroscopy with digital imaging, enables both spatial and spectral information, allowing its potency to describe the distribution of constituents within a sample [16]. For instance, IR–HSI has been used for detecting adulteration in tuber flour [17], sorghum [18], wheat [19], and meat [2,20,21].

Usually, detection of adulteration using IR–HSI is modelled using partial least square regression (PLSR), which uses the entire full waveband spectra. However, variable-waveband selection methods can be used to identify spectral variables. with significant contributions to the performance of the model, improving computational efficiency and reducing computer memory. One method is Variable Importance in Projection (VIP), which uses scores to evaluate the importance of each variable in a PLSR model [22]. Therefore, this study compares PLSR models constructed using full waveband and VIP selected spectra in predicting pork in minced beef.

2. Materials and Methods

2.1. Meat Sample Preparation

Beef and pork minced meat were purchased from a meat supplier named Meat Club Store in Yuseong, Daejeon, South Korea. The meats were minced again in the laboratory to achieve uniformity. Minced pork with concentrations of 2%, 5%, 10%, 20%, 30%, 40%, and 50% (w/w) were added to minced beef, making a total of 70 g per sample, which were then thoroughly mixed, placed on a 90 mm × 15 mm petri dish, and stored in a refrigerator at 10 °C. Prior to spectral acquisition, the meat samples were conditioned at room temperature. By taking photos of samples using a DLSR camera (Canon EOS 700D, Tolyo, Japan), the Red–Green–Blue (RGB) images of pure minced beef and pork, as well as pork adulterated beef, are shown in Figure 1. Analysis of Figure 1 reveals that the presence of pork in meat is difficult to distinguish using the naked eye, although, there was a clear difference between pure beef and pork. Therefore, hyperspectral image analysis will be employed to overcome these limitations.

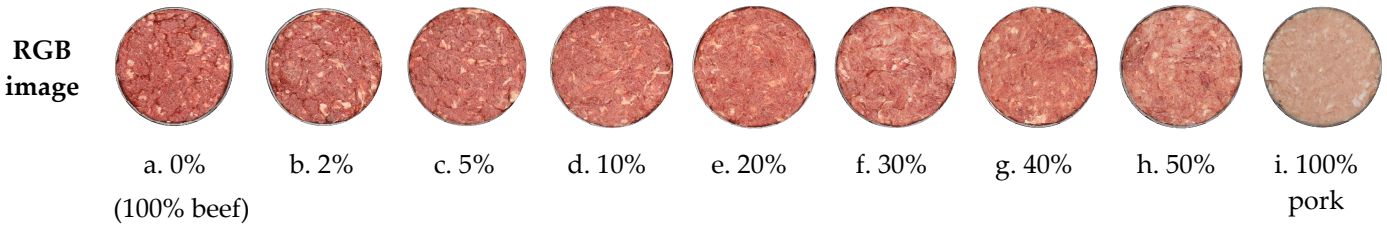

Figure 1. RGB images of pure minced beef and pork and pork adulterated beef samples in various percentage concentrations of pork.

2.2. Hyperspectral Image Acquisition

This research used the line-scan SWNIR–HSI instrument, the same system reported by [2]. The system consisted of a line-scan camera system (Headwall Photonics, Fitchburg, MA, USA) with a mercury cadmium telluride (MCT) detector (Xeva-2.5-320, Xenics, Heverlee, Belgium) and six tungsten–halogen lamps (100 W, 12 V, Light Bank; JCR 12V, Ushio Inc., Tokyo, Japan). The SWNIR–HSI covers 894–2504 nm attaining 275 spectral variables. The sample was placed on the platform moved by a DC motor at a speed of 3.48 mm/s with 600 scans per sample. Prior to sample scanning, the dark reference images were obtained by closing the camera lens and turning the light off to set a 0% reflectance, while the white reference, using the white Teflon board-images, was obtained to set a 100% reflectance. It is important to note that the halogen lamps were preheated at least 15 min before measurement, ensuring stable illumination during data collection. Moreover, since halogen lamps generate heat, which can negatively influence the spectra quality, the room used for measurement was kept cool. Two dishes of samples for each concentration of pork meat (Figure 1) were scanned to obtain hyperspectral images in 3D hypercubes with two spatial x and y coordinates and wavelength variables (λ), resulting in final dimensions of 384 (x) × 550 (y) × 275 (λ).

2.3. Chemical Analysis

Although the chemical compositions of meat were not extensively discussed, proximate analysis was conducted to obtain comprehensive results. The proximate compositions were measured after acquiring the hyperspectral images. In summary, the moisture, protein, fat, and ash contents of the samples were analyzed using standard laboratory methods described by [2]. Moisture was determined by drying the samples in an oven, protein by measuring nitrogen content using the Kjeldahl method, fat by extraction with ether, and ash by burning the samples in an oven. The proximate data are presented in Table 1.

Table 1. The proximate contents of meat samples. Data are from reference [2], with permission from Elsevier.

Proximate Parameter	Beef	Pork
Moisture (%)	72.45 ^{b}	71.00 ^{a}
Crude protein (%)	22.35 ^{c}	19.56 ^{a}
Crude fat (%)	4.12 ^{a}	7.27 ^{c}
Crude ash (%)	1.07 ^{a}	1.27 ^{b}

$^{a–c}$ Mean values within each row with different superscripts are significantly different (Sig. < 0.05).

2.4. Data Analysis

The workflow of this research is illustrated in Figure 2. The workflow for developing a PLSR model to predict the concentration of pork adulteration in minced beef begins with spectra acquisition, spectra extraction, spectra preprocessing, and PLSR model development, using full wavelengths and VIP-selected wavelengths.

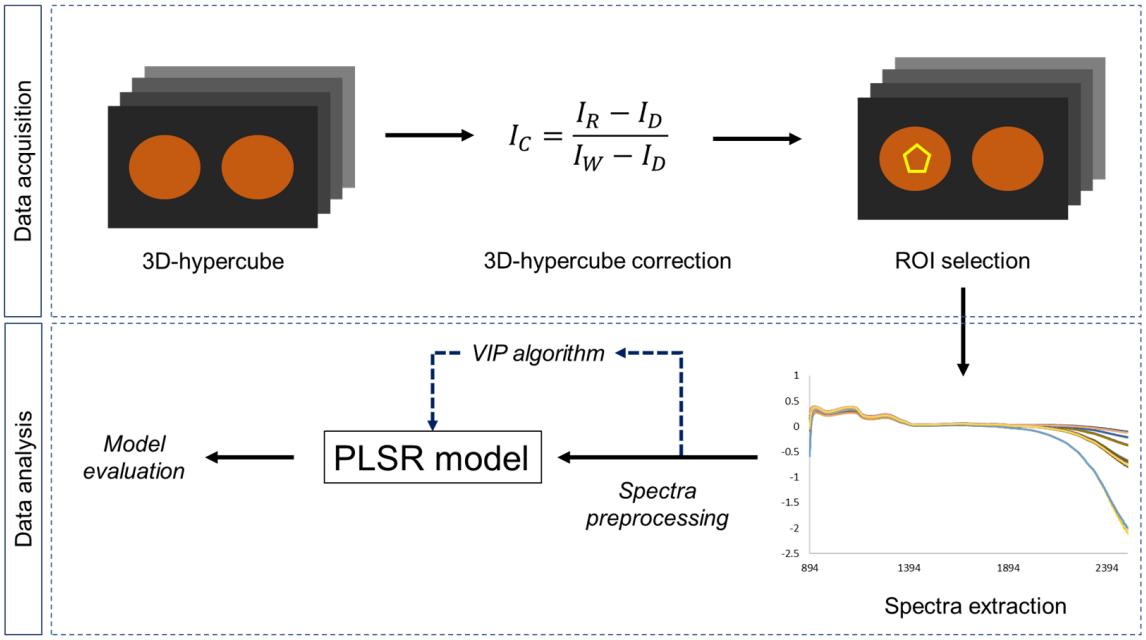

Figure 2. Workflow for developing a PLSR model to predict concentration of pork adulteration in minced beef, which begin with spectra acquisition, spectra extraction, spectra preprocessing, and PLSR model development, using full wavelengths and VIP-selected wavelengths.

2.4.1. Spectra Data Extraction

Three-dimension (3D) reflectance images were obtained from the SWNIR–HSI system. Reflectance spectra were obtained by creating a polygon of the region of interest (ROI) in the x–y space. To eliminate background pixels, the threshold value was set to 0.2. Pixels of the spectra in the ROI were averaged to obtain one spectrum. The spectrum that shows the difference between background and sample was chosen to obtain x–y data. In this study, the selected spectra were 1141.5 nm. The extraction of spectra was performed using MATLAB® (R2018a, The MathWorks, Inc., Natick, MA, USA). All the spectra data were transformed to MS Excel® and then imported to MATLAB® for spectra preprocessing and multivariate analysis.

2.4.2. Spectra Preprocessing

Apart from sample information, the data acquired from the spectrometer, including the SWNIR–HSI, contain noises that might be affected by scattering, which occurs when the light waves interact with tiny particles in the samples. To obtain reliable, accurate and stable calibration models, spectra preprocess are required before modeling [23]. Spectra preprocessing methods can be classified into scatter correction and spectral derivative methods [24]. In this study, PLSR models were developed using original (raw) spectra and spectra obtained from various preprocessing methods, such as Max normalization, Range normalization, Standard normal variate (SNV), multiplicative scatter correction (MSC), and Savitzky–Golay 1st and Savitzky–Golay 2nd Derivatives.

2.4.3. Partial Least Square Regression (PLSR) Analysis

PLSR analysis was used to develop models for predicting the concentration of minced pork adulteration in minced beef. Of all spectra data, 60% and 40% of the data were used for calibration and prediction, respectively. The PLSR includes two variables, i.e., reflectance spectra as predictors (x-variables) and concentrations of pork as response (y-variables). The PLSR algorithm converts the predictor and the response into new variables, namely latent variables (LVs); hence, it is crucial to find the optimum number of LVs. During

the PLSR calibration, 18 LVs were set as the initial value. Herein, we did not apply too many LVs at initial value, to avoid overfitting; indeed, a higher number of LVs might provide good accuracy, but increase the complexity of the model. At the same time, a full cross-validation, i.e., leave-one-out cross-validation (LOOCV), was also used to avoid overfitting. The selection of best LVs was carried out by considering the local minimum of mean square error (MSE), while serving the cumulative explained variance in Y by at least 85%. Finally, the optimum LVs was re-applied to the PLSR model and the prediction calculated using the formula outlined in Equation (1). In Equation (1), y_p is concentration of pork; X_i is reflectance value from the SWNIR–HSI instrument; β_i is regression (beta) coefficient value; and ϵ is bias.

$$y_p = \sum_{i=1}^{n} X_i \beta_i + \epsilon \quad (1)$$

Apart from using all or full wavelengths for developing PLSR models to predict concentrations of pork, the Variable importance in the projection (VIP) method was used to reduce variables in developing the model. The computation of the VIP score was generated from the PLSR algorithm to reduce useless information and improve estimation accuracy, stability, and operation efficiency [25]. Furthermore, wavelength with VIP score > 1 was considered as the influential wavelength in predicting percentage of pork in beef.

The PLSR models' accuracy was evaluated based on the coefficient of determination of calibration (R^2_C) and prediction (R^2_P) (Equation (2)), and standard error of calibration (SEC) and prediction (SEP) (Equation (3)). The $y_{a,i}$ is the actual value of concentrations of pork at every i-th row; n is number of the samples; and $\overline{y}_a$ is the average actual value of concentration of pork.

$$R^2 = 1 - \frac{\sum_{i=1}^{n} \left(y_{a,i} - y_{p,i}\right)^2}{\sum_{i=1}^{n} \left(\overline{y}_a - y_{a,i}\right)^2} \quad (2)$$

$$SE = \sqrt{\frac{1}{n-1} \sum_{i=1}^{n} \left(y_{a,i} - y_{p,i} - \left(\frac{1}{n} \sum_{i} y_{p,i} - y_{a,i} \right) \right)^2} \quad (3)$$

3. Results and Discussion

3.1. Spectra Analysis

Figure 3 illustrates the representative NIR spectrum from the ROI preprocessed with the Savitzky–Golay first derivative. Accordingly, various peaks and valleys were observed, spanning from 894 nm to 2500 nm, mainly characterized by XH chemical bonds [26]. One study reported that meat is comprised of typical macromolecules, such as protein, lipid, water, and carbohydrate [27]. The peaks in the region within 894 nm to 1000 nm are assigned with OH bonds related to the water molecules in meat samples [27]. Various peaks between 1000 and 1500 nm were also observed, corresponding with the CH_2 bond, which may refer to fat [28]. However, no distinct signatures appeared between 1500 nm and 2000 nm, while other peaks were distinguishable beyond 2000 nm. The peaks from 2200 nm to 2500 nm are responsible for the protein content [2]. Overall, the spectral pattern of the samples was relatively similar, making them difficult to distinguish solely on spectra information; thereby, multivariate analysis is necessary to facilitate the quantification of the adulterant content, which in this case was pork.

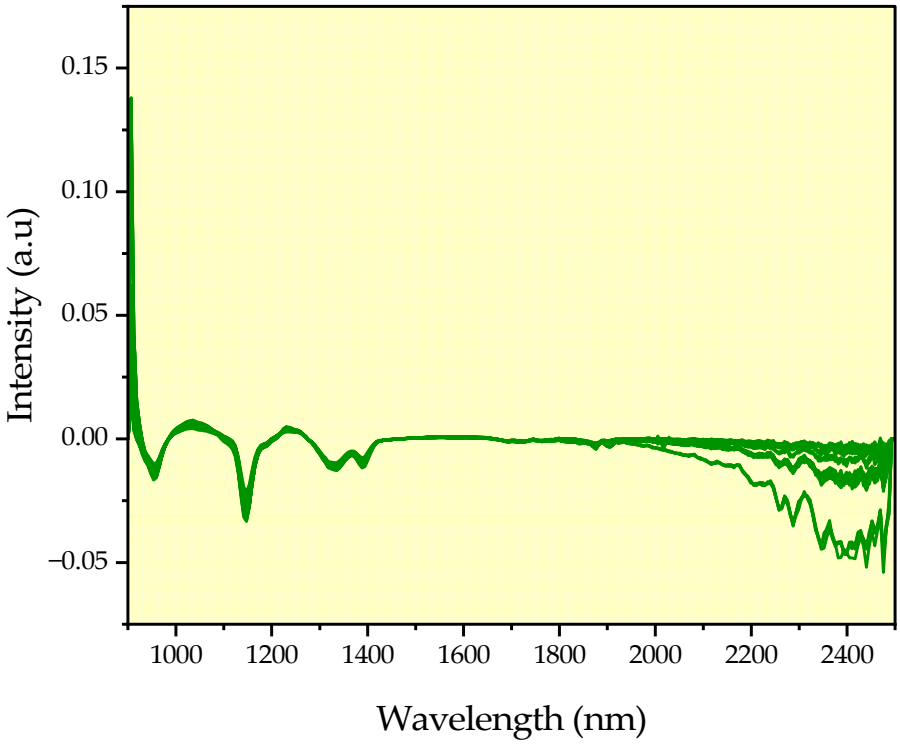

Figure 3. NIR spectra of selected ROI processed with Savitzky–Golay first derivative.

3.2. PLSR Using the Full Range

PLSR was used to develop a model based on the hundreds of variables from the hyperspectral imaging data [29]. In PLSR, there is a linear relationship between the predictor (spectral data) and the response (pork levels). The performance of PLSR in predicting pork levels in beef using the full range spectrum is listed in Table 2.

Table 2. Evaluation performance of full wavelength PLSR using original and preprocessed spectra.

Preprocessing	R^2_C	SEC (%)	R^2_P	SEP (%)	LVs
Max normalization	0.926	4.834	0.909	5.384	4
Range normalization	0.856	6.726	0.864	6.995	5
MSC	0.832	7.263	0.814	7.770	3
SNV	0.895	5.754	0.870	6.513	5
Savitzky–Golay 1st	0.979	2.568	0.940	4.633	4
Savitzky–Golay 2nd	0.975	2.811	0.910	5.913	4
Raw	0.972	2.968	0.937	4.572	5

Based on Table 2, for the calibration model, PLSR exhibited an R^2_C ranging from 0.832 to 0.979 with an SEC ranging from 2.568–6.726%, similar to the study of Silva et al. [27]. It can be seen that the Savitzky–Golay first derivative preprocessing achieved the highest calibration accuracy (R^2c = 0.979 and SEC = 2.568%), underlining its effectiveness in capturing significant spectral features. The results indicate that calibration performance depends on preprocessing methods. Using prediction data sets that were not used in developing calibration models, PLSR models resulted in R^2p values ranging from 0.814 to 0.940, with SEP values between 4.633% and 7.770%. Using four latent variables (LVs), spectra preprocessed with the Savitzky–Golay first derivative achieved the highest prediction accuracy, yielding an R^2_P of 0.940 and SEP of 4.633%. The results confirmed the reliability of the Savitzky–Golay first derivative for practical applications. Although using raw spectra without preprocessing was able to detect the pork adulteration percentage, the R^2c was

lower, and SEC and LV were higher than with Savitzky–Golay first derivative. In contrast, the preprocessing method using MSC revealed the lowest performance, with lower R^2c and R^2p values and higher SEC and SEP, suggesting its limitations in managing spectral variation. In the previous study, Savitzky–Golay first derivative working with PLSR generated the optimum model (R^2_P of 0.90 and SEP of 0.118 mg/g) in predicting cyanidine-3-glucoside in soybean seeds using FT–NIR spectroscopy [30]. Likewise, Savitzky–Golay first derivative resulted in deep learning prediction performance in estimating wine grape berries pH (RMSEP of 0.11) and sugar (RMSEP of 0.755 °Brix) content, in conjunction with hyperspectral imaging [31]. Poor results in PLSR using MSC may be due to the inability of MSC to effectively handle overlapping absorbance peaks, as MSC performs well only when chemical variations are smaller than physical light scattering variations [32], which is not the case with the complex chemical components in minced pork and beef.

In order to find the most significantly contributing wavelengths, a beta coefficient from the optimum model was evaluated in this study (Figure 4). Four wavelengths, positioned at 1065 nm, 1165 nm, 1300 nm, and 2417 nm, were those making strong contributions. Wavelengths at 1065 and 1165 nm were assigned with amines characterized by C–N, C–H, and NH_2 bonds [27]. Another study revealed that the band at around 1150 nm C–H was due to fat. Furthermore, an absorption band located at 1300 nm was due to the fat molecule (C–H bond), as cited elsewhere in our previous study [2]. On the other hand, the last absorption band, i.e., 2417 nm, was due to the N–H in protein [33]. Accordingly, these peaks might be caused by the changes in chemical properties caused by adulteration.

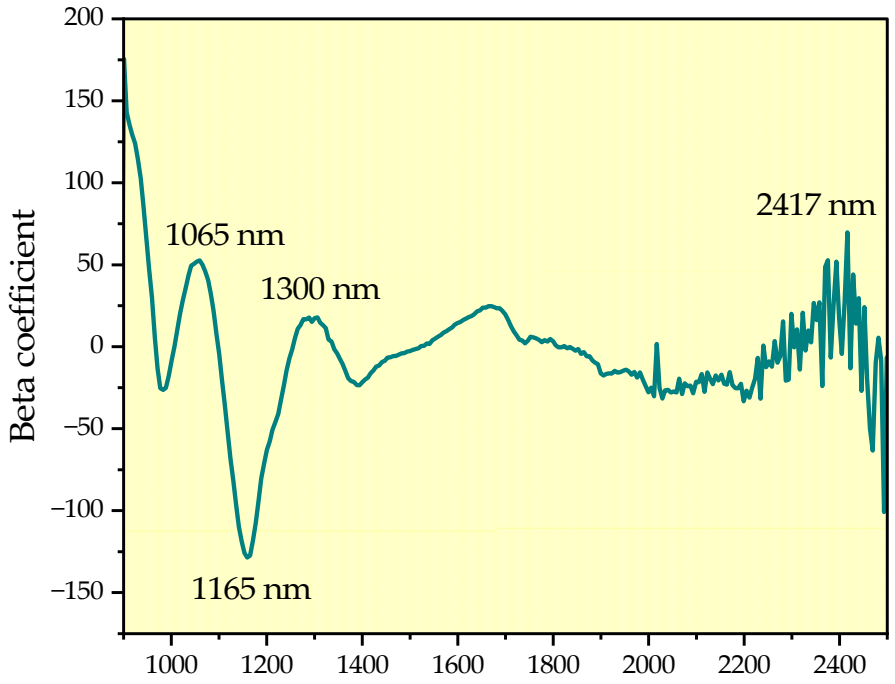

Figure 4. The beta coefficient curve generated from the optimum model.

3.3. PLSR Using VIP Selected Wavelengths

Based on the previous sections, the PLSR using full wavelength included 275 variables in model calibration. However, multicollinearity may still occur between variables, e.g., wavelength, causing difficulty for the model in finding which wavelength contributed to predicting pork levels. Thus, this paper investigated a reconstructed PLSR model using a selected wavelength extracted from the VIP algorithm. Ninety (90) effective wavebands were successfully extracted by applying "1" as the cut-off value, such that the wavelength

with the VIP score < 1 was considered as a variable with low contribution and discarded from the original matrix (Figure 5).

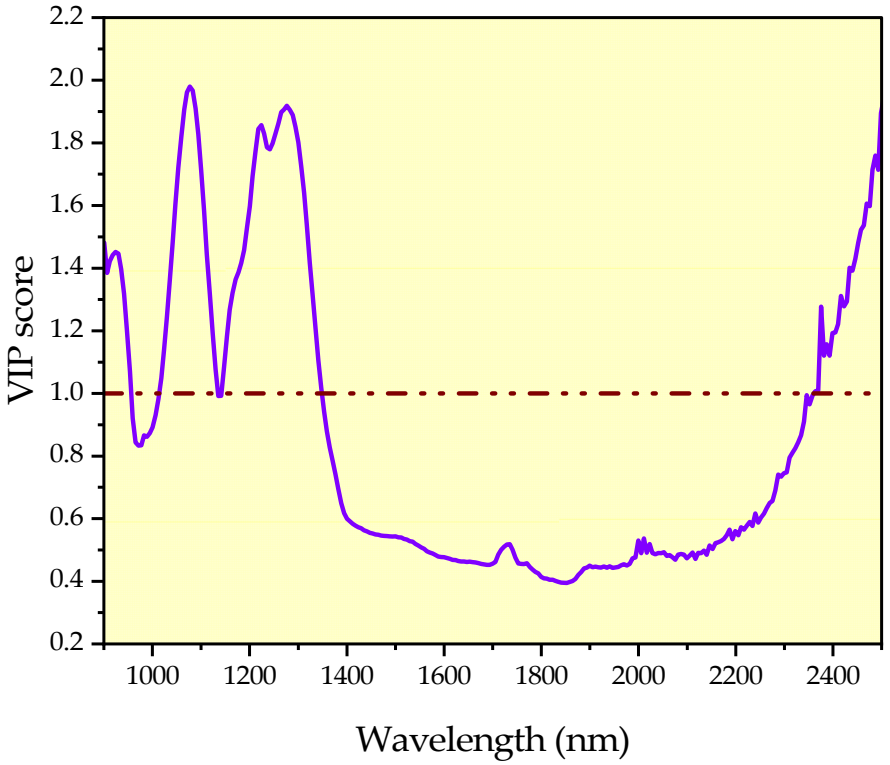

Figure 5. VIP calculation result. The red line indicates the cut-off value.

Table 3 shows the performance of PLSR models developed using calibration data sets, which resulted in acceptable performance, denoted by R^2_C of 0.826–0.969 with an SEC ranging from 3.137% to 7.386%, slightly close to the performance of PLSR using full wavelength (Table 2). Based on Table 3, the Savitzky–Golay first derivative demonstrated the highest R^2c (0.973) and the lowest SEC (2.884%), indicating a robust calibration model, while the MSC process again exhibited lower R^2c (0.826) and higher SEC (7.386%). After the prediction data sets were applied to the best Savitzky–Golay first derivative PLSR model, it produced an R^2_P of 0.929 and an SEP of 4.914%.

Table 3. Evaluation performance of selected wavelength PLSR using original and preprocessed spectra.

Preprocessing	R^2_C	SEC (%)	R^2_P	SEP (%)	LVs
Max normalization	0.945	4.151	0.935	4.634	5
Range normalization	0.876	6.246	0.866	6.985	5
MSC	0.826	7.386	0.823	7.765	3
SNV	0.912	5.243	0.870	6.717	5
Savitzky–Golay 1st	0.973	2.884	0.929	4.914	4
Savitzky–Golay 2nd	0.969	3.137	0.901	6.059	4
Raw	0.969	3.140	0.955	3.811	5

The new PLSR model developed using VIP selection (Table 3) was comparable with the original PLSR model (Table 2) in terms of the high coefficient of determination (R^2) and the low standard error (SE). The VIP selection was able to reduce from 275 to 90 variables, which provides a fast process and less computer memory required for computation. The finding can be used to develop a spectral system with a few wavelengths, which can reduce device cost and increase production line speed to fulfill the requirements of the food

industry [34]. Other studies confirmed the use of VIP variable selection, which improves the PLSR model for adulteration detection [14,35].

4. Conclusions

The study examined the performance of NIR hyperspectral imaging in terms of its feasibility in predicting pork levels in beef. A traditional multivariate analysis, PLSR, facilitated the predictive model using full and effective wavelengths. Using full wavelength (275 wavelengths), the PLSR model generated an R^2_P of 0.814–0.940 with a SEP of 4.633–7.770%. The optimum PLSR model using full wavelength was achieved by using Savitzky–Golay first derivative preprocessed spectra, yielding R^2_P of 0.940 and SEP of 4.633%. A VIP algorithm was used to select the effective wavelengths and applied "1" as a cut-off value, resulting in 90 effective wavelengths. The PLSR was redeveloped using 90 wavelengths, yielding an R^2_P of 0.955 with an SEP of 3.811% by original spectra. Our study demonstrated that PLSR using 90 wavelengths could enhance the performance of PLSR using full wavelength. Therefore, NIR hyperspectral imaging with selected wavelengths could be a good tool for rapid and nondestructive identification of pork levels.

The utilization of PLSR as traditional machine learning for spectral data analysis has been continuously employed and shows good prediction accuracy. However, the limitation of the PLSR is in using the assumption of linearity between the spectral and the reference matrix, in this case pork concentration. However, there might be a linear relation between the spectral and pork concentration, the condition during measurement, e.g., the scattering effect may cause non-linearity [36]. Therefore, utilizing a non-linear model, such as deep learning, support vector machine, decision tree, etc., could be an alternative to overcome the problem, as these models are more flexible. Furthermore, since hyperspectral imaging provide spatial information, it might be possible to conduct the analysis at the pixel level, finding the pork pixel concentration. Exploration of an on-line hyperspectral imaging system is also possible regarding practical aspects (the sorting process).

Author Contributions: Conceptualization, R.E.M.; methodology, R.E.M.; formal analysis, R.E.M. and H.Z.A.; investigation, R.A.P.H., M.F.R.P. and J.K.; resources, B.-K.C.; writing—original draft preparation, R.E.M. and R.A.P.H.; writing—review and editing, R.E.M. and B.-K.C.; funding acquisition, R.E.M. All authors have read and agreed to the published version of the manuscript.

Funding: This research was funded by the Ministry of Education, Culture, Research, and Technology of Indonesia, grant number 122/E5/PG.02.00.PL/2023 and 3170/UN1/DITLIT/DitLit/PT.01.03/2023.

Data Availability Statement: The raw data supporting the conclusions of this article will be made available by the authors on request.

Acknowledgments: The author thanks the Department of Smart Agriculture Systems and the Department of Biosystems Machinery Engineering, College of Agricultural and Life Science, Chungnam National University, Korea for allowing us to use the SWNIR–HSI system during the experiment.

Conflicts of Interest: The authors declare no conflicts of interest.

References

1. Momtaz, M.; Bubli, S.Y.; Khan, M.S. Mechanisms and Health Aspects of Food Adulteration. *Foods* **2023**, *12*, 199. [CrossRef] [PubMed]
2. Masithoh, R.E.; Pahlawan, M.F.R.; Kim, J.; Arief, M.A.A.; Kurniawan, H.; Hernanda, R.A.P.; Amanah, H.Z.; Cho, B.K. Shortwave infrared hyperspectral imaging for the determination of pork adulteration in minced beef and lamb. *Food Control* **2024**, *166*, 110736. [CrossRef]

3. Zahroh, A.; Fahri, M.; Pahlawan, R.; Rahmawati, L. Application of visible and shortwave near infrared spectroscopy combined with PCA-LDA and PLS-DA to distinguish sirloin and shank beef. In Proceedings of the 3rd International Conference on Smart and Innovative Agriculture; Sumantyo, J., Ed.; Atlantis Press International BV: Dordrecht, The Netherlands, 2022; pp. 392–399.
4. Meza-Márquez, O.G.; Gallardo-Velázquez, T.; Osorio-Revilla, G. Application of mid-infrared spectroscopy with multivariate analysis and soft independent modeling of class analogies (SIMCA) for the detection of adulterants in minced beef. *Meat Sci.* **2010**, *86*, 511–519. [CrossRef] [PubMed]
5. Leng, T.; Li, F.; Xiong, L.; Xiong, Q.; Zhu, M.; Chen, Y. Quantitative detection of binary and ternary adulteration of minced beef meat with pork and duck meat by NIR combined with chemometrics. *Food Control* **2020**, *113*, 107203. [CrossRef]
6. Kucharska-Ambrożej, K.; Karpinska, J. The application of spectroscopic techniques in combination with chemometrics for detection adulteration of some herbs and spices. *Microchem. J.* **2019**, *153*, 104278. [CrossRef]
7. Golinelli, L.P.; Carvalho, A.C.; Casaes, R.S.; Lopes, C.S.C.; Deliza, R.; Paschoalin, V.M.F.; Silva, J.T. Sensory analysis and species-specific PCR detect bovine milk adulteration of frescal (fresh) goat cheese. *J. Dairy Sci.* **2014**, *97*, 6693–6699. [CrossRef]
8. Yamamoto, K.; Yahada, A.; Sasaki, K.; Funakoshi-Yoshida, A.; Ohta, C.; Koga, N.; Ohta, H. Detection of adulterated shiikuwasha juice by sensory evaluation, colorimetric value and volatile components. *Food Sci. Technol. Res.* **2013**, *19*, 843–848. [CrossRef]
9. Cuadros-Rodríguez, L.; Ruiz-Samblás, C.; Valverde-Som, L.; Pérez-Castaño, E.; González-Casado, A. Chromatographic fingerprinting: An innovative approach for food "identitation" and food authentication—A tutorial. *Anal. Chim. Acta* **2016**, *909*, 9–23. [CrossRef]
10. Sobrino-Gregorio, L.; Vilanova, S.; Prohens, J.; Escriche, I. Detection of honey adulteration by conventional and real-time PCR. *Food Control* **2019**, *95*, 57–62. [CrossRef]
11. Masithoh, R.E.; Roosmayanti, F.; Rismiwandira, K.; Pahlawan, M.F.R. Detection of Palm Sugar Adulteration by Fourier Transform Near-Infrared (FT-NIR) and Fourier Transform Infrared (FT-IR) Spectroscopy. *Sugar Tech* **2022**, *22*, 920–929. [CrossRef]
12. Rismiwandira, K.; Roosmayanti, F.; Pahlawan, M.F.R.; Masithoh, R.E. Application of Fourier Transform Near-Infrared (FT-NIR) Spectroscopy for Detection of Adulteration in Palm Sugar. In *IOP Conf Series: Earth and Environmental Science*; IOP Publishing Ltd.: Purwokerto, Indonesia, 2020; p. 012122.
13. Roosmayanti, F.; Rismiwindira, K.; Masithoh, R.E. Detection of coconut (*Cocos nucivera*) sugar adulteration in palm (*Arenga pinnata* Merrill) sugar by Fourier Transform Infrared (FT-IR) Spectroscopy. *Food Res.* **2021**, *5*, 31–36. [CrossRef]
14. Masithoh, R.E.; Amanah, H.Z.; Cho, B.K. Application of fourier transform near-infrared (FT-NIR) and fourier transform infrared (FT-IR) spectroscopy coupled with wavelength selection for fast discrimination of similar color of tuber flours. *Indones. J. Chem.* **2020**, *20*, 680–687. [CrossRef]
15. Lee, H.; Cho, B.K.; Kim, M.S.; Lee, W.H.; Tewari, J.; Bae, H.; Sohn, S.I.; Chi, H.Y. Prediction of crude protein and oil content of soybeans using Raman spectroscopy. *Sens. Actuators B Chem.* **2013**, *185*, 694–700. [CrossRef]
16. Manley, M. Near-infrared spectroscopy and hyperspectral imaging: Nondestructive analysis of biological materials. *Chem. Soc. Rev.* **2014**, *43*, 8200–8214. [CrossRef]
17. Masithoh, R.E.; Kandpal, L.M.; Lohumi, S.; Yoon, W.S.; Amanah, H.Z.; Cho, B.K. Shortwave Infrared Hyperspectral Imaging for the Determination and Visualization of Chemical Contents of Wheat and Tuber Flour. *Int. J. Adv. Sci. Eng. Inf. Technol.* **2022**, *12*, 1574–1579. [CrossRef]
18. Bai, Z.; Hu, X.; Tian, J.; Chen, P.; Luo, H.; Huang, D. Rapid and nondestructive detection of sorghum adulteration using optimization algorithms and hyperspectral imaging. *Food Chem.* **2020**, *331*, 127290. [CrossRef]
19. Verdú, S.; Vásquez, F.; Grau, R.; Ivorra, E.; Sánchez, A.J.; Barat, J.M. Detection of adulterations with different grains in wheat products based on the hyperspectral image technique: The specific cases of flour and bread. *Food Control* **2016**, *62*, 373–380. [CrossRef]
20. Jia, W.; Ferragina, A.; Hamill, R.; Koidis, A. Modelling and numerical methods for identifying low-level adulteration in ground beef using near-infrared hyperspectral imaging (NIR-HSI). *Talanta* **2024**, *276*, 126199. [CrossRef]
21. Kamruzzaman, M.; Sun, D.W.; ElMasry, G.; Allen, P. Fast detection and visualization of minced lamb meat adulteration using NIR hyperspectral imaging and multivariate image analysis. *Talanta* **2013**, *103*, 130–136. [CrossRef]
22. Gorji, R.; Skvaril, J.; Odlare, M. Determining Moisture Content of Basil Using Handheld Near-Infrared Spectroscopy. *Horticulturae* **2024**, *10*, 336. [CrossRef]
23. Cen, H.; He, Y. Theory and application of near infrared reflectance spectroscopy in determination of food quality. *Trends Food Sci. Technol.* **2007**, *18*, 72–83. [CrossRef]
24. Rinnan, Å.; van den Berg, F. Review of the most common preprocessing techniques for near-infrared spectra. *TrAC Trends Anal. Chem.* **2009**, *28*, 1201–1222. [CrossRef]
25. Yun, Y.H.; Li, H.D.; Deng, B.C.; Cao, D.S. An overview of variable selection methods in multivariate analysis of near-infrared spectra. *TrAC Trends Anal. Chem.* **2019**, *113*, 102–115. [CrossRef]

26. Amanah, H.Z.; Rahayoe, S.; Harmayani, E.; Hernanda, R.A.P.; Khoirunnisaa Rohmat, A.S.; Lee, H. Construction of a sustainable model to predict the moisture content of porang powder (*Amorphophallus oncophyllus*) based on pointed-scan visible near-infrared spectroscopy. *Open Agric.* **2024**, *9*, 20220268. [CrossRef]
27. Silva, L.C.; Folli, G.S.; Santos, L.P.; Barros, I.H.; Oliveira, B.G.; Borghi, F.T.; dos Santos, F.D.; Filgueiras, P.R.; Romao, W. Quantification of beef, pork, and chicken in ground meat using a portable NIR spectrometer. *Vib. Spectrosc.* **2020**, *111*, 103158. [CrossRef]
28. Cozzolino, D.; Murray, I. Identification of animal meat muscles by visible and near infrared reflectance spectroscopy. *LWT Food Sci. Technol.* **2004**, *37*, 447–452. [CrossRef]
29. Lee, H.; Kim, M.S.; Lim, H.S.; Park, E.; Lee, W.H.; Cho, B.K. Detection of cucumber green mottle mosaic virus-infected watermelon seeds using a near-infrared (NIR) hyperspectral imaging system: Application to seeds of the "Sambok Honey" cultivar. *Biosyst. Eng.* **2016**, *148*, 138–147. [CrossRef]
30. Amanah, H.Z.; Joshi, R.; Masithoh, R.E.; Choung, M.G.; Kim, K.H.; Kim, G.; Cho, B.K. Nondestructive measurement of anthocyanin in intact soybean seed using Fourier Transform Near-Infrared (FT-NIR) and Fourier Transform Infrared (FT-IR) spectroscopy. *Infrared Phys. Technol.* **2020**, *111*, 103477. [CrossRef]
31. Gomes, V.; Mendes-Ferreira, A.; Melo-Pinto, P. Application of hyperspectral imaging and deep learning for robust prediction of sugar and ph levels in wine grape berries. *Sensors* **2021**, *21*, 3459. [CrossRef]
32. Jochemsen, A.; Alfredsen, G.; Martens, H.; Burud, I. Exploring the use of extended multiplicative scattering correction for near infrared spectra of wood with fungal decay. *Chemom. Intell. Lab. Syst.* **2024**, *252*, 105187. [CrossRef]
33. Maduro Dias, C.S.A.M.; Nunes, H.P.; Melo, T.M.M.V.; Rosa, H.J.D.; Silva, C.C.G.; Borba, A.E.S. Application of Near Infrared Reflectance (NIR) spectroscopy to predict the moisture, protein, and fat content of beef for gourmet hamburger preparation. *Livest. Sci.* **2021**, *254*, 104772. [CrossRef]
34. Oliveira, M.M.; Ferreira, M.V.S.; Kamruzzaman, M.; Barbin, D.F. Prediction of impurities in cocoa shell powder using NIR spectroscopy. *J. Pharm. Biomed. Anal. Open* **2023**, *2*, 100015. [CrossRef]
35. Oussama, A.; Elabadi, F.; Platikanov, S.; Kzaiber, F.; Tauler, R. Detection of olive oil adulteration using FT-IR spectroscopy nd PLS with variable importance of projection (VIP) scores. *J. Am. Oil Chem. Soc.* **2012**, *89*, 1807–1812. [CrossRef]
36. Liu, A.; Li, G.; Fu, Z.; Guan, Y.; Lin, L. Non-linearity correction in NIR absorption spectra by grouping modeling according to the content of analyte. *Sci. Rep.* **2018**, *8*, 8564. [CrossRef]